Engineered Science
DOI: https://dx.doi.org/10.30919/es1388

Optimal Headlamp Adjustment for Vehicles through Slip Angle and Stiffness Analysis using Dynamic Vehicle Model

Glenson Toney,[1, 2,*] Gaurav Sethi[1] and Cherry Bhargava[3]

Abstract

The current research presents a novel non-linear method for optimizing headlight adjustment using vehicle dynamic modeling. The study describes the vehicle models and gives a MATLAB-based mathematical model that is used to control the headlight adjustment. The dynamic vehicle-based model employs a slip angle evaluation technique to create a state space model that accurately determines the difference between the vehicle's position and the location of the headlight. The calculation of longitudinal and lateral velocity, and the yaw rate around the Center of Gravity, is critical to the model's capacity to predict the slip angle and, thus, govern the headlight angle. The model is deduced from differential equations and governed by Newton's law of motion. Furthermore, the study examines the effect of body stiffness, which is a crucial factor to consider when cornering, and the model achieves acceptable results within the allowable stiffness range for passenger vehicles. The simulation of the model against the car body angle shows the effective adjustment of the headlamp according to the varying degree of cornering, thus assisting in headlamp adjustment to improve ride comfort, providing strong evidence for its potential to significantly improve driving safety and comfort by optimizing headlamp adjustment. The model's consideration of body stiffness also ensures that it will contribute to the improvement of steering and vehicle handling.

Keywords: Vehicle dynamic modeling; Slip angle: Body stiffness; State space model.
Received: 18 April 2023; Revised: 29 August 2023; Accepted: 04 September 2023.
Article type: Research article.

1. Introduction

Driving at night or in adverse weather can be arduous owing to the limited vision which can compromise driving safety. The primary source of visibility while driving is headlamps, which illuminate the road ahead and allow drivers to anticipate and react to obstacles. Conventional headlamp systems are meant to offer a fixed beam pattern, but they fail to adjust to varying driving conditions, such as turns, slopes, and oncoming traffic, leading to potential hazards. Consequently, adaptive headlamp systems have emerged as a potential solution to enhance driving safety and comfort.[1] Adaptive headlamps utilize advanced sensing technologies, such as cameras and radar, to evaluate driving conditions and modify the light beam pattern accordingly. They can adjust the headlamp's direction, intensity, and spread to illuminate the driver's path optimally, irrespective of driving conditions. Such systems have been shown to enhance visibility, reduce glare, and improve reaction times, all of which contribute to safer driving. The need for adaptive headlamp systems is further emphasized by research on driving safety, which indicates that inadequate visibility is a significant contributor to road accidents, especially during nighttime or adverse weather conditions. Therefore, the incorporation of adaptive headlamps in vehicles is crucial to ensure driving safety and reduce the risk of accidents.[1] Time gap platooning systems for vehicle transportation also offer a promising capability for communicating between cars and adjusting headlamps accordingly.[2-4]

Vehicle mathematical modeling is predominantly used in the design of adaptive headlamp controllers and it is diverse: geometric path tracking,[5] Kinematics and extended kinematics model,[6-13] Pure pursuit model,[14-18] Vector pursuit model,[19] Clothoid Curve method.[20] Without the requirement for factors like velocity or other external variables, geometric path tracking models a vehicle by using its position, size, look ahead of the trajectory, and orientation. This model has a

[1] *School of Electronics and Electrical Engineering, Lovely Professional University, Phagwara, Punjab, 144411, India*
[2] *Department of Electronics and Communication Engineering, St Joseph Engineering College, Vamanjoor, Mangaluru, Karnataka, 575028, India*
[3] *Department of Computer Science and Engineering, Symbiosis International University, Pune, Maharashtra, 412115, India*
**Email:* glensherton@gmail.com (G. Toney)

complexity in the look-ahead-distance selection, which, at a greater distance, bypasses the path's corners and ends up at the new location directly. The Kinematic model does not require consideration of internal or external forces but instead makes use of the vehicle's location and acceleration with respect to the coordinates (local and global). The front steerable wheels are taken into account as fixed coordinates in the absolute model using the bicycle model, with the front axle serving as the origin.[6-9] To make the model suitable for linear and rotational motion with substantially improved stability, many controllers were devised.[10,11] In contrast to the earlier model, the extended Kinematic model also takes tire slip, coupling,[12] and coefficient of friction into account.[13] The pure pursuit model defines a circular arc between the location where the vehicle is currently located and the eventual destination indicated by the look ahead to determine the error between the goal of the direction in which the vehicle is traveling.[14] The dependence on look-ahead distance limits its usage for adaptive headlamp vehicle model design. The vector pursuit takes advantage of the coordinate system to forecast the orientation needed to reach the endpoint, which might be employed in adaptive headlights, but its usage is limited by the computing cost. The Clothoid Curve approach avoids the arc, operates in real-time, and offers more consistent performance.[19] The force acting owing to ground and tire contact, as well as the longitudinal and lateral forces acting on the wheel, are also used in the dynamic route tracking approach.[21]

1.1 Slip angle assessment to determine the deviation between the vehicle's position and the headlamp's location

Slip angle is the difference between the true heading (the direction in which the vehicle's body is pointing) and the direction in which it is moving (also referred to as true heading or course over). A positive slip angle refers to a tire moving to the right as it advances in the positive direction. The SAE Tire Axis system depicts the slip angle (α) and its indication of the desired and the true heading of the vehicle's body,[22] and Fig. 1 depicts how the slip angle is the measure of this difference. As seen in Fig. 1, even if the wheel is turned to make the turn, the body of the vehicle is still pointed away from the intended trajectory. The headlamp will also illuminate the true heading rather than the actual direction of travel as a result of this.

Since the slip angle is a clear indication of this variance, it can be used to calculate how much the vehicle is deviating from its intended course and to adjust for the direction of the headlamps. When a car is turning, it can either perform a regular maneuver or oversteer or understeer. In each of these three scenarios, the body slip angle continues to be a reliable indicator of the difference between the true heading and the direction of travel; therefore, this was taken into account while designing the model to modify the headlight adjustment in this study to enhance road lighting when turning. Slip angle has been found effective in predicting the vehicle trajectory where the error of prediction is as low as 0.3 m.[23] It is known that as a vehicle rotates, there is a mismatch between the velocity vector's directions and the heading angle, which is the slip angle. This serves as a gauge for determining the vehicle traversal path. Typical techniques for the traditional calculation of the slip angle include the direct integration method and the linear observer estimation method.[24-27] These studies have referred to the effective calculation of slip angle, which can aid in predicting the difference between the actual and required path and hence, adjust the headlamp.

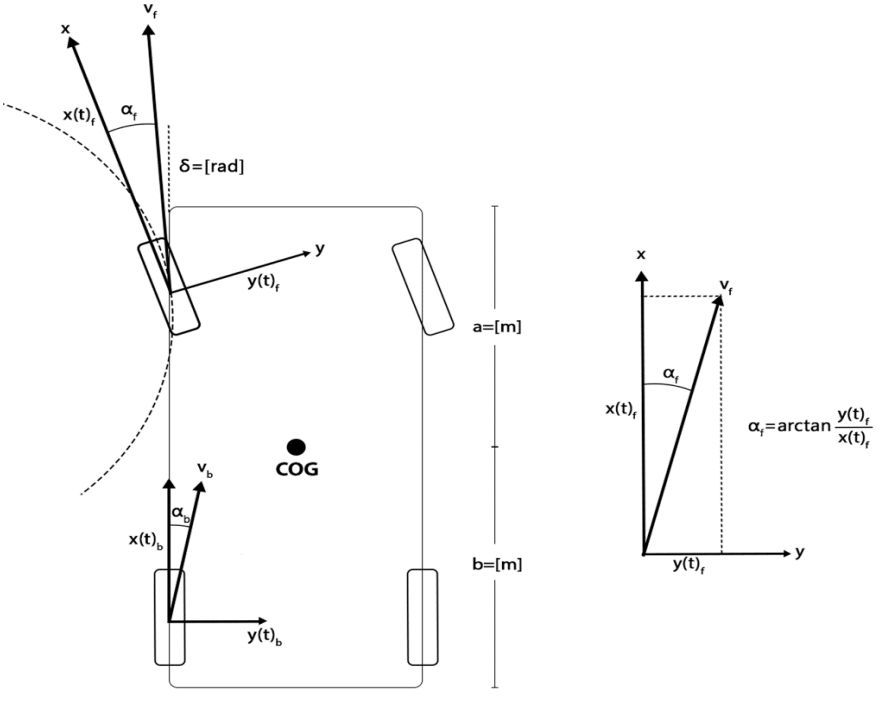

Fig. 1: Slip angle at the front and rear wheels as vehicle performs a cornering where α_f represents the front slip and $\alpha_b$the back/ rear slip. When $\alpha_f > \alpha_b$ vehicle undergoes an understeer, when $\alpha_f < \alpha_b$ vehicle is oversteering and $\alpha_f = \alpha_b$ represents a neutral state.

This work discusses vehicle mathematical modeling using dynamic vehicle modeling, which is appropriate for analyzing slip angles. It allows for the examination of it and the stiffness of a vehicle at any time throughout its operation. The stiffness and/or tilt of a vehicle can be represented as a function of speed using dynamic vehicle modeling. The primary advantage of dynamic modeling is its inherent ability to analyze the performance of different tires under various types of driving conditions by changing either the angle or stiffness, as well as the ability to determine the vehicle response to dynamic loadings such as acceleration and cornering. The purpose of this work is to create a state space model for adaptive headlight systems in vehicles using dynamic modeling in MATLAB. This has the potential to substantially improve driving safety and comfort. The mathematical model is designed largely with the vehicle slip angle and stiffness in mind, which can contribute to the improvement of vehicle engineering and lead to the construction of technologies that assure safe driving.

2. Mathematical modeling

2.1 Mathematical model for measuring the body slip angle and headlamp adjustment

The model employs the law of motion (Newton's) and basic geometric relations to express the longitudinal velocity, the lateral velocity, and r(t), the yaw rate, which are measured with respect to Center-Of-Gravity (COG), via three differential equations.[28] The paper also investigates the impact that body stiffness has on steering, handling, and ride comfort. Dynamic Vehicle model is used to design the model.[29] The steering wheel's rotation is transformed into a linear motion that turns the wheels and directs the trajectory. Based on these, the directions can be divided into three categories: front, center, and back, and the angles are predicated on each of them, and then the body slip angle for each category.

2.2 Methodology

The Lateral and longitudinal velocities and the yaw rate, which depend on the front, the center, and the rear angles of the vehicle, enable the body slip-angle computation. While designing the state space model that predicts the body-slip angle, the paramount is on these parameters. The headlamp adjustment is completed by calculating the actual deflection of the right and left headlamp and adjusting it according to the slip angle as depicted in the workflow in Fig. 2. The body stiffness (B) of a vehicle influences the slip angle during cornering, whether the vehicle is experiencing normal, under, or oversteering. Hence, the work has a state space model that considers the body stiffness factor. This model can be used for controller development.

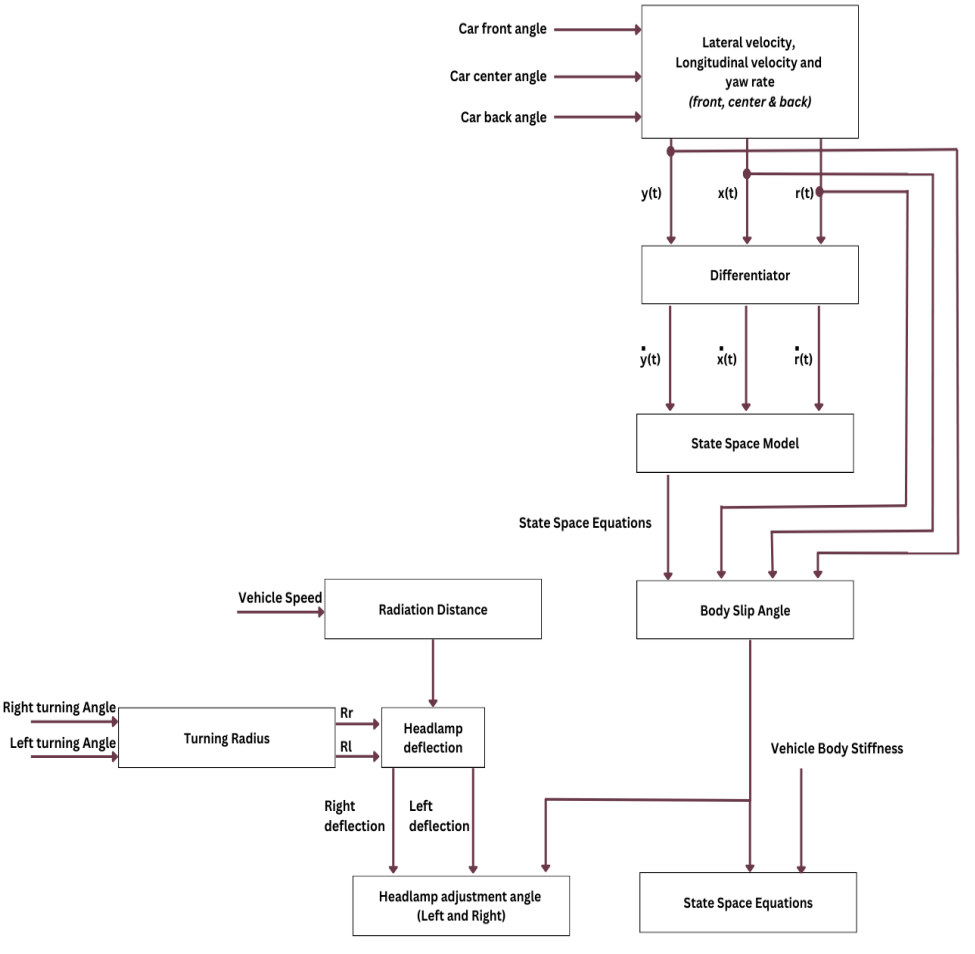

Fig. 2: The flow of slip angle-based headlamp adjustment.

2.3 The body slip angle and headlamp adjustment model

Dynamic vehicle models are reasonable and applicable approximations for passenger cars and the research work has developed the slip angle-based headlamp control (non-linear, grey-box) using this model. Here the tire forces are considered to be linear and the stiffness parameter, both longitudinal and lateral for all four tires are assumed to be the same. The slip at the front wheel is calculated considering the slip at the rear to be non-existent because the model intends to calculate the front slip and hence predict the headlamp deviation from the actual path. The model considers the impact of Body Stiffness of the passenger vehicle whose effect becomes pronounced during cornering.

Notations

θ_f: Car front angle
θ_c: Car center angle
θ_b: Car back angle
v: Speed of the Car
COG: Center of Gravity
BS_f: Body Slip Angle, Front
BS_c: Body Slip Angle, Center
BS_b: Body Slip Angle, Back
y(t): lateral velocity
x(t): longitudinal velocity
r(t): Yaw rate
CA: Air Resistance Coefficient= 0.5
m: mass =1292.2 kg
J: Moment of inertia= 2380.7 kgm^2
a and b: distances from the Center of Gravity to the front and rear axles= 1.5 m
t: turning angle
S: Radiation distance
R: Turning radius
D: Vehicle wheelbase
δ_l andδ_r: Turning angle of left and right, respectively
HL_l and
HL_r: headlamp left and right adjustments, respectively
B: Car body stiffness
$\frac{dv_{x(t)}}{dt}, \frac{dv_{y(t)}}{dt}, \frac{dr(t)}{dt}$: first order differential equation in longitudinal, lateral, and yaw.

The slip angle is proportional to the ratio of lateral velocity and longitudinal velocity. These are dependent on the velocity of the vehicle and the vehicle's body angle. The longitudinal velocity, lateral velocity, and yaw rate observed around the Center of Gravity (COG) of the vehicle may be described by three differential equations using Newton's law of motion and certain fundamental geometric relationships as depicted in equations 1 through 3. Considering the Mass = 1292.2 kg, Inertia =2380.7kgm^2,[9] and an Air resistance coefficient CA=0.5, the differential values are computed. The drag coefficient of the typical modern car ranges from 0.25 to 0.3. Due to their often boxy forms, sport utility vehicles (SUVs) typically achieve a coefficient of 0.35-0.45. The body design of a vehicle has an impact on its drag coefficient. While research on Indian budget automobiles reveals that this number can reach as high as 0.7 for a few, it often ranges between 0.4 and 0.7, contrary to what the automotive industry typically claims for a drag coefficient of 0.3 and below.[30-33] In this paper, a nominal value of 0.5 is used in consideration of Indian subcontinent passenger cars.

$$\frac{dv\_x(t)}{dt} = y(t)_f \times r(t) + \frac{1}{m}[(x(t)_f \times \cos(t)) - (y(t)_f \times \sin(t))] + x(t)_b - CA \times x(t)_f^2 \quad (1)$$

$$\frac{dv\_y(t)}{dt} = -x(t)_f \times r(t) + \frac{1}{m}[(x(t)_f \times \sin(t)) - (y(t)_f \times \cos(t))] + y(t)_b \quad (2)$$

$$\frac{dr(t)}{dt} = \frac{1}{J} * [a(x(t)_f) \times \sin(t)] - [(y(t)_f \times \cos(t))] - b \times y(t)_b \quad (3)$$

where t is the steering angle (0^o to 30^o), v_x(t) denotes that the force along the longitudinal direction acts on the x-axis, while v_y(t) denotes that it is along the y-axis. $x(t)_f$, $y(t)_f$ represents the car front longitudinal and lateral components respectively. The air resistance term, which is considered to be a quadratic function of the longitudinal vehicle velocity v_x(t), is included in the first equation that describes the longitudinal acceleration. The state space matrix for calculating the body slip angle is derived and represented by equations 4 and 5. The State Space Model structure, along with the impact of the Body Stiffness factor, is derived from solving the differential Eqs. 1-3 and represented using Eqs. 4-8.

$$\begin{bmatrix}\dot{x}(t)\\ \dot{y}(t)\\ \dot{r}(t)\end{bmatrix} = \begin{bmatrix}0 & 1 & 1\\ -1 & 0 & 1\\ \alpha & 0 & 0\end{bmatrix}\begin{bmatrix}x(t)_f\\ y(t)_f\\ r(t)_f\end{bmatrix} + \begin{bmatrix}\frac{1}{m}\cos(t) & \frac{1}{m}\sin(t) & \frac{1}{J}\end{bmatrix}\begin{bmatrix}x(t)_f\\ y(t)_f\\ r(t)_f\end{bmatrix} \quad (4)$$

$$Y = \begin{bmatrix}1 & -b & 0\end{bmatrix}\begin{bmatrix}x(t)_b\\ y(t)_b\\ r(t)_b\end{bmatrix} + \begin{bmatrix}CA & 0 & 0\end{bmatrix}\begin{bmatrix}x(t)_f\\ y(t)_f\\ r(t)_f\end{bmatrix} \quad (5)$$

$$\frac{dx_1(t)}{dt} = \frac{dv\_y(t)}{dt} \times \frac{dr(t)}{dt} + \frac{1}{m}[B(BS_f \times \cos(t))] - 2 \times \left[B \times \frac{\left(t - \left(\frac{dv\_y(t)}{dt} + a \times \frac{dr(t)}{dt}\right)\right)}{\left(\frac{dv\_x(t)}{dt} \times \sin(t)\right)}\right] + B \times (BS_c) - CA \times \frac{dv\_x(t)^2}{dt} \quad (6)$$

$$\frac{dx_2(t)}{dt} = \frac{dv\_x(t)}{dt} \times \frac{dr(t)}{dt} + \frac{1}{m}[B(BS_f \times sin(t))] + 2 \times \left[B \times \frac{\left(t - \left(\frac{dv\_y(t)}{dt} + a \times \frac{dr(t)}{dt}\right)\right)}{\left(\frac{dv\_x(t)}{dt} \times cos(t)\right)}\right] + 2 \times B \times (BS_c) - CA \times \frac{dv\_x(t)^2}{dt} \quad (7)$$

$$\frac{dx_3(t)}{dt} = \frac{1}{\left((0.5 \times (a+b))\right)^2 \times m}\left(a \times \left(B \times (BS_f \times \sin(t))\right) + 2 \times$$

$$B\left(\left(t-\left(\frac{dv\_y(t)}{dt}+a\times\frac{dr(t)}{dt}\right)/\frac{dv\_x(t)}{dt}\right)\right)\times\cos(t)-2\times b\times B\left(b\times\frac{dr(t)}{dt}-\left(\frac{dv\_x(t)}{dt}/\frac{dv\_y(t)}{dt}\right)\right) \quad (8)$$

Using the state space model equations, the Body slip angle is calculated using Eqs. 9-14.

$$y_1(t)=x_1(t) \quad (9)$$

$$y_2(t)=\frac{1}{m}\left(B\times\left(\frac{dv_{x(t)}}{dt}\times\sin(t)\right)\right)+2\times B\left(t-\left(\frac{dv\_y(t)}{dt}+a\times\frac{dr(t)}{dt}\right)\right)/\frac{dv\_x(t)}{dt} \quad (10)$$

$$y_3(t)=x_3(t) \quad (11)$$

$$BS_f=\frac{y(t)_f}{x(t)_f} \quad (12)$$

$$BS_c=\frac{y(t)_c}{x(t)_c} \quad (13)$$

$$BS_b=\frac{y(t)_b}{x(t)_b} \quad (14)$$

The Body slip gives an estimate of the intended path to travel, and it is important for us to calculate the current position of the headlamp, which is calculated in the next section. The radiation distance and the turning angle, in turn, decide this angle. The calculations are defined through Eqs. 15-18 where v is the velocity, δ_l & δ_r are the left and right turning angle, and D is the vehicle wheel base.

The Radiation distance is computed taking into account the vehicle speed as

$$S=0.0094v^2+0.6057v+3.1730 \quad (15)$$

The turning radius of a car depends on the wheel and is computed as

$$R_l=D/\sin\delta_l \quad (16)$$

$$R_r=D/\sin\delta_r \quad (17)$$

The deflection of the headlamp angle is computed as

$$\Theta=\arcsin(S/2R) \quad (18)$$

Based on the deflection angle both left and right headlamps are adjusted. The head lamp adjustments are represented as shown in Eqs. 16 and 17.

$$HL_l=BS_f-\Theta_l \quad (19)$$

$$HLr=BS_f-\Theta_r \quad (20)$$

The state space equations for the headlamp adjustment are derived through Eqs. 18-23 as follows:

$$dx[0]=\frac{dx_2(t)}{dt}\times\frac{dx_3(t)}{dt}+\frac{1}{m}\times B\times BS_f\times\cos(t)-2\times B\times\left(\left(t-\left(\frac{dx_2(t)}{dt}+a\times\frac{dx_3(t)}{dt}\right)\right)/\left(\frac{dx_2(t)}{dt}\right)\times\sin(t)\right) \quad (21)$$

$$dx[1]=-\frac{dx_1(t)}{dt}\times\frac{dx_3(t)}{dt}+\frac{1}{m}\times(B\times BS_c)\times\sin(t)+2\times B\times\left(\left(t-\frac{dx_2(t)}{dt}+a\times\frac{dx_3(t)}{dt}\right)/\frac{dx_1(t)}{dt}\right)\times\cos(t)+2\times B\times\left(\left(t-\frac{dx_1(t)}{dt}+a\right)\times\frac{dx_3(t)}{dt}/\frac{dx_1(t)}{dt}\right)\times\cos(t)+2\times B\times b\times\left(\frac{dx_3(t)}{dt}-\frac{dx_2(t)}{dt}\right)/\frac{dx_1(t)}{dt} \quad (22)$$

$$dx[2]=2^{\frac{(a+b)}{2}}\times m\times(a\times B\times BS_f\times\sin(t))+2\times B\times\left(t-\left(\frac{dx_2(t)}{dt}+a\right)\times\frac{dx_3(t)}{dt}/\frac{dx_1(t)}{dt}\right)\times\cos(t)-2\times b\times B\times\left(b\times\frac{dx_3(t)}{dt}/\frac{dx_1(t)}{dt}\right) \quad (23)$$

$$y[0]=x[0] \quad (24)$$

$$y[1]=\frac{1}{m}\times B\times BS_f\times\sin(t)+2\times B\times\left(t-\left(\frac{dx_2(t)}{dt}+a\right)\times\frac{dx_3(t)}{dt}/\frac{dx_1(t)}{dt}\right)\times\cos(t)+2\times B\times\left(b\times\frac{dx_3(t)}{dt}-\frac{dx_2(t)}{dt}\right)/\frac{dx_1(t)}{dt} \quad (25)$$

$$y[2]=x[2] \quad (26)$$

3. Results and discussion

The state space model is designed to improve the illumination of the intended path of travel during cornering which otherwise leads to over or under-steer due to errors in judgment on the angle of cornering. The model primarily depends on the prediction of the angle at which the vehicle is turning. An effective metric to calculate the desired path travel is the Body Slip angle. The calculation of the body slip angle to differentiate between the vehicle's true heading and that of the direction in which the body is pointing involves the retrieval of the car front, center and back angle to define the longitudinal and lateral velocities.[26] These calculations aid in determining the actual headlamp position and the intended position and hence can be compensated.

Another important metric to be considered for the effectiveness of the developed model is the performance against the body stiffness of the vehicle.[33-35] This is crucial as the stiffness factor has a predominant effect during vehicle cornering and the model is developed for headlamp adjustment during the cornering.

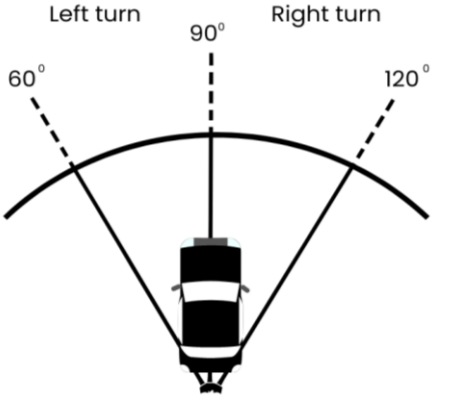

Fig. 3: The range of steering angle for a right and left cornering.

The headlamp adjustments are evaluated on multiple cases: a left turn and a right turn. The steering angle limit is 0.5 radian, which is a maximum of 30°. The left turn from the COG is considered 90° to 60° while the right turn is 90° to 120° as shown in Fig. 3. The effectiveness of the model is in detecting the corresponding slip angles and adjusting the headlamp beams. The model developed shows promising results in this range for the body stiffness in the range of passenger cars. The complete range of simulation values can be found in Table S1 of the supplementary files. The longitudinal and lateral velocities of front, back and center are determined and the slip angle is tabulated using the State space model designed in Section 2. Based on the slip angle the car headlamp is adjusted with respect to the car body direction.

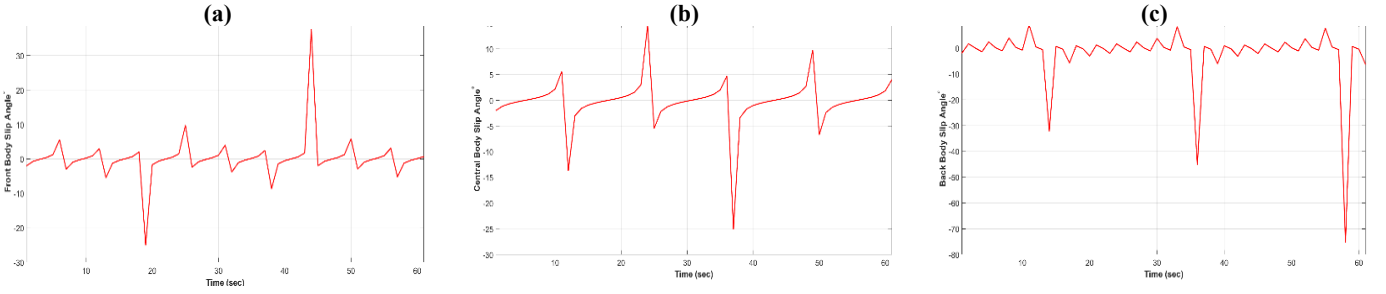

Fig. 4: Body slip angle of (a) front, (b) center, and (c) back.

3.1 Case 1: Vehicle taking a right turn (from the center to the right side (90° to 120°)

Fig. S1 displays the analysis of the lateral velocity of the car's front direction, as it turns from 90 to 120 degrees to the right, with each degree of lateral velocity being measured. Similarly, Fig. S2 illustrates the analysis of longitudinal velocity from 90 to 120 degrees of turning. Based on the front lateral and longitudinal values, the slip angle of the car body is analyzed and tabulated from 90 to 120 degrees of turning, as illustrated in Fig. 4(a). Furthermore, the car center lateral velocity is determined and plotted from the turning angle of 90 to 120 degrees in Fig. S3, while the corresponding longitudinal velocity is computed and plotted in Fig. S4 for the turning angle of 90 to 105 degrees.[20,21] Using the lateral and longitudinal velocities of the car's center velocity, the body slip angle is determined, and the observed values are graphically represented in Fig. 4(b).

Similarly, the back lateral velocity is computed at the turning degree of 90 to 30 degrees, and it is illustrated in Fig. S5. The respective formula examines the longitudinal velocity of the car's back for the turning degree of 90 to 30 degrees and the graphical representation of the backside longitudinal velocity is depicted in Fig. S6. The car's back slip angle is computed using both the lateral and longitudinal velocities, and it is illustrated in Fig. 4c. Subsequently, the longitudinal, lateral, and yaw rate values are differentiated with respect to time. The longitudinal, lateral, and yaw rate of the car when turning to the right is depicted in Figs. S7-S9, respectively. Finally, the deflection of the headlamp is determined using radiation distance and turning radius. The deflection of both the right and left headlamps is different and is illustrated in Figs. 5(a) and 5(b), respectively. The headlamp is adjusted separately using the deflection angle of the lamp and the body slip angle. As the values of deflection are dissimilar, the adjustment of the lamp is not the same for both lamps. The adjustments of the right and left side lamps are shown in Figs. 6(a) and 6(b), respectively. However, upon analysis, it is observed that the variation between the left and right headlamp position adjustments is minimal and almost negligible, making the transition on both ends almost identical.

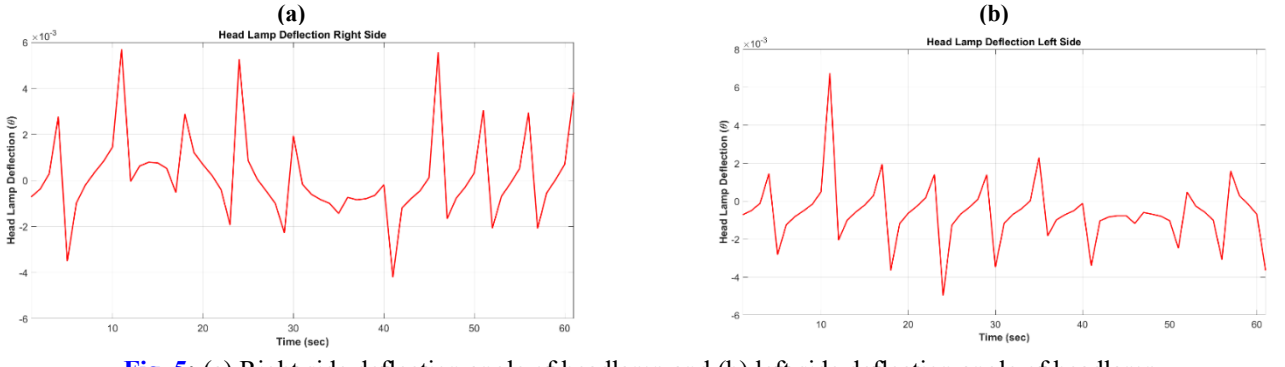

Fig. 5: (a) Right side deflection angle of headlamp and (b) left side deflection angle of headlamp.

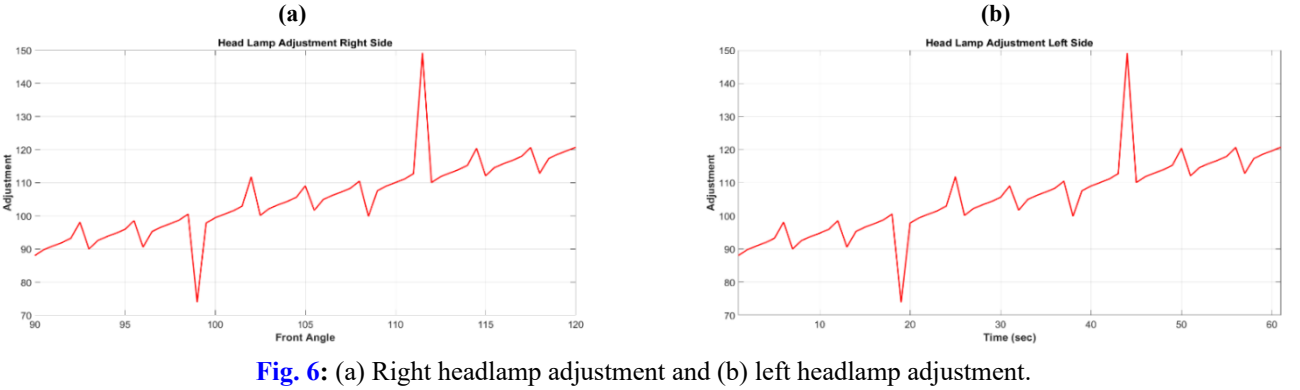

Fig. 6: (a) Right headlamp adjustment and (b) left headlamp adjustment.

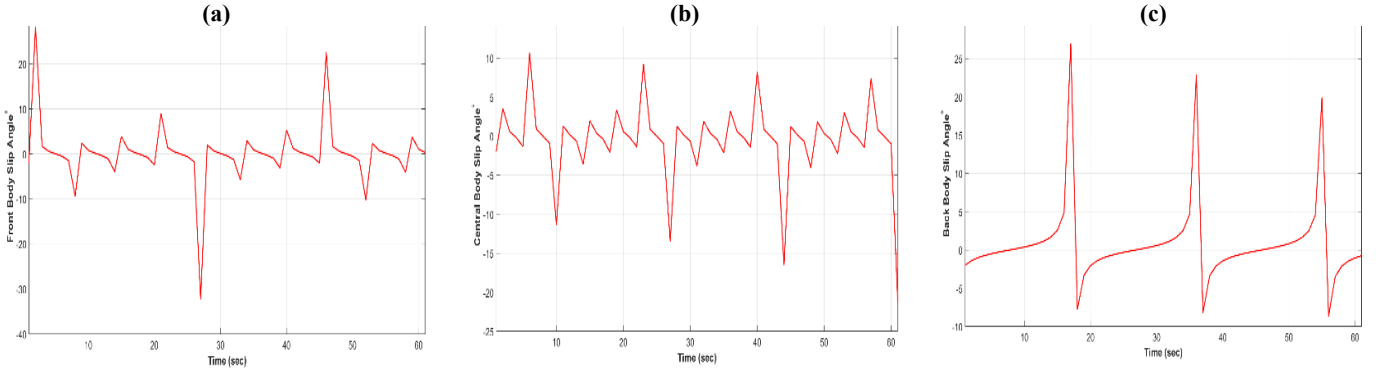

Fig. 7: Body slip angle of (a) front, (b) center, and (c) back.

3.2 Case 2: Vehicle taking a Left turn (from the center to the left side (90º to 60º)

Let us assume the turning angle of the car (left side).[36,37]

θ_f = 90º to 60º, θ_c = 90º to 45º, and θ_b = 90º to 100º

Turning angle: Left = 90 to 30.68ºand Right = 90 to 42.65º

In this study, the determination of the lateral, longitudinal, and yaw rate of a vehicle is investigated using a specified parameter value. Based on these parameters, the slip angle of the vehicle (Fig. 7) and the deflection of a lamp are computed and used to adjust the headlamp. The results are presented in Figs. S10 and S11 and Fig. 8(a), which illustrate the lateral velocity, longitudinal velocity, and slip angle of the car's front. The lateral and longitudinal velocities are calculated by substituting the vehicle speed and direction into a specified formula. Using these values, the slip angle of the vehicle is determined, as depicted in Fig. 7 for left-side turns. Similarly, the lateral velocity, longitudinal velocity, and yaw rate of the car's center section are computed, with this section varying from 90 degrees to 45 degrees. From these degrees, the slip angle of the vehicle is calculated, as shown in Figs. S12, S13 and Fig. 7. The lateral and longitudinal velocities of the car's rear section are also computed, with this section turning from 90 degrees to 100 degrees during left-side turns. The results are plotted in Figs. S14, and S15. Finally, the body slip angle of the vehicle is determined and presented in Fig. 7.

Upon determining the slip angle, the differentiation of lateral, longitudinal, and yaw rates is computed using Newton's law. The observed values of these parameters are plotted in Figs. S16-S18. Subsequently, the headlamp deflection is computed using the differentiation values of lateral, longitudinal, and yaw rates. Both left and right-side headlamp deflections are determined and provided in Fig. 8(a) and 8(b), respectively. The headlamp of the car is then adjusted using the deflection and slip angle of the front part of the vehicle. The lateral and longitudinal velocities are updated every second, and the slip angle of the car is computed at the specified time period using these values. Both the slip angle and deflection angle of the car are used to adjust the headlamp with respect to the car direction. The adjustments of the right and left side headlamps are plotted in Figs. 9(a) and 9(b), respectively.

3.3 Adjustment versus direction of a car

This section presents the comparison between the degree of car headlamp adjustment and the direction of car movement. Specifically, the adjustment of the car headlamp during a left turn, ranging from 90° to 60°, and a right turn, ranging from 90° to 120°, is examined. The corresponding values of headlamp adjustment against the vehicle front angle for left cornering are depicted separately in Fig. 10(a) and Fig. 10(b), while the right turn in Fig. 11(a) and Fig. 11(b), respectively. Fig. 12(a) and Fig. 12(b) provide a combined representation of the adjustment degree of the left and right headlamps and the

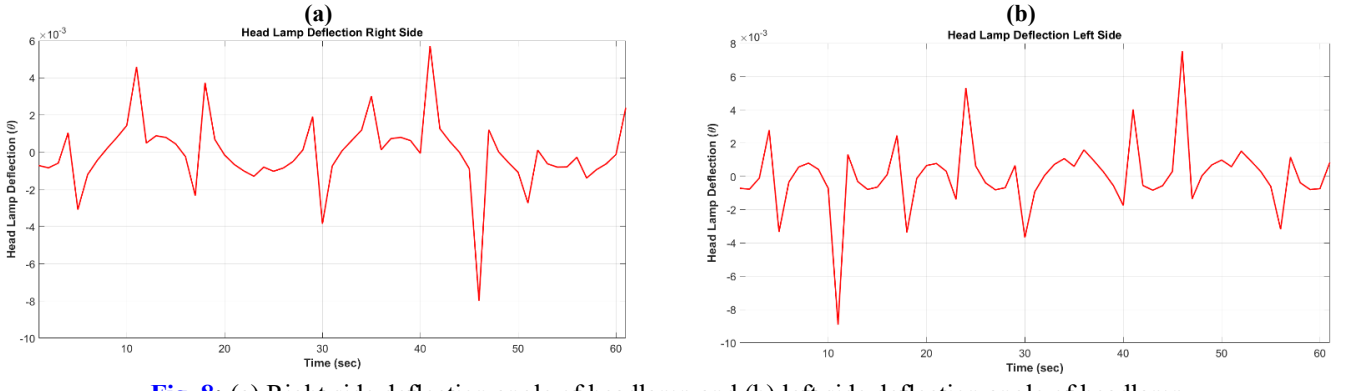

Fig. 8: (a) Right side deflection angle of headlamp and (b) left side deflection angle of headlamp.

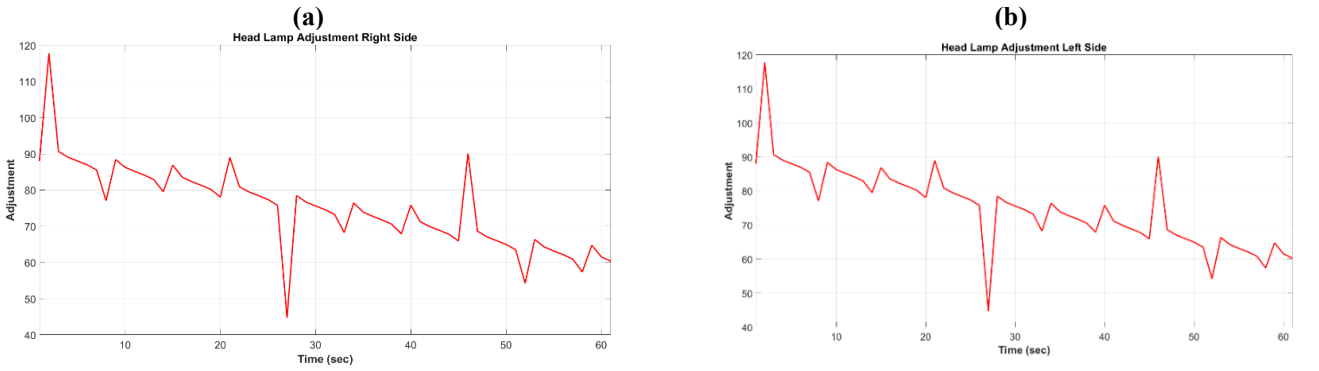

Fig. 9: (a) Right headlamp adjustment and (b) left headlamp adjustment.

car's front angle against the slip angle that is calculated using the lateral and longitudinal velocities and the yaw rate of the vehicle, respectively. Table S1 tabulates the right and left headlamp adjustments based on the vehicle front angle, which is, in turn, deduced through the slip angle. 60° represents the left extreme turn, while 120° represents the right extreme. The values from the left extreme to the right extreme with an increment of 0.5° are shown in Table S1. From these plots, it can be observed that the adjustment degree of the headlamps is synchronized with the slip angle of the vehicle.

This suggests that the headlamp adjustment mechanism is designed to compensate for any deviation between the actual position of the vehicle and the location of the headlamps, thereby ensuring that the road ahead is illuminated effectively. This synchronization between the headlamp adjustment and the slip angle calculation is vital for safe and efficient driving, especially in low light or adverse weather conditions where proper illumination of the road is critical for maintaining visibility and avoiding accidents. The results presented in these figures demonstrate the effectiveness of the proposed method for adjusting the headlamp position in response to changes in the vehicle's position and direction, thereby improving the overall safety and performance of the vehicle.

3.4 Body stiffness (B) and its effect on the model

Predominantly important specification of the passenger car, which affects not just the weight but also the fuel consumption along with its handling, steering, and ride characteristics, is Body Stiffness.[33] Research has shown that as the body stiffness (B) increases, the flexibility of the car body becomes the primary factor affecting the ride. This influence is more related to geometry-based filtering than the natural frequency (bogie), which can lead the vehicle into resonant vibrations that may be catastrophic.[37] Flexural-mode shapes of the body are found to have an effect on comfort at lower frequencies.[38] Studies prove the fact that both the stiffness and the damping parameters of the vehicle suspension greatly influence ride comfort.[39] A stiffer body aids in keeping the wheels aligned during cornering. By reducing the chassis' flexing and twisting, it enables more direct steering input transmission to the wheels. As a result, the steering system is more accurate and sensitive, giving the driver greater control of the car. Studies suggest that body stiffness affects vehicle steering by influencing on-center handling, steering response, suspension geometry, and steering return ability, with factors such as torsion bar stiffness, cornering stiffness, and steering system parameters playing significant roles.[40,41]

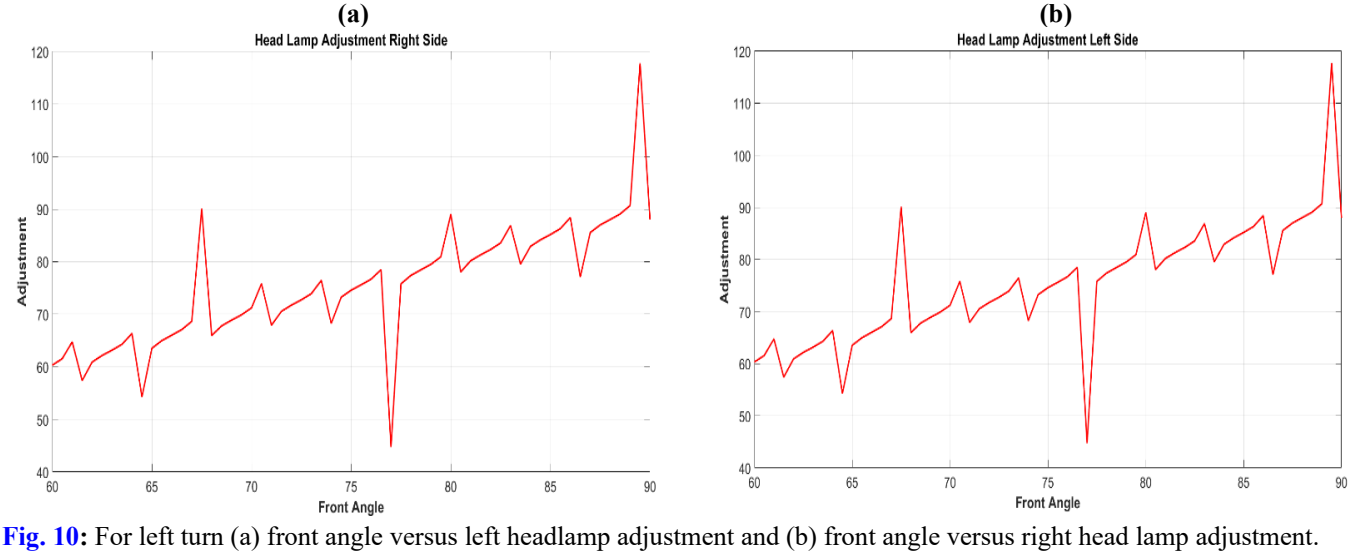

Fig. 10: For left turn (a) front angle versus left headlamp adjustment and (b) front angle versus right head lamp adjustment.

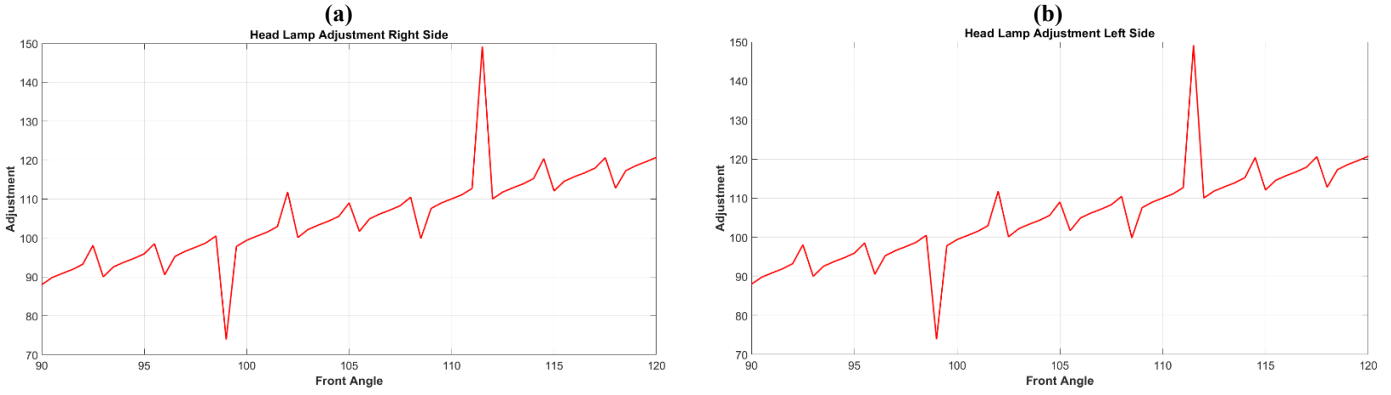

Fig. 11: For right turn (a) front angle versus left headlamp adjustment and (b) front angle versus right head lamp adjustment

Body stiffness is essential for preserving a vehicle's stability and control (handling) during cornering and other dynamic maneuvers. Body roll, the sideways tilting motion of the vehicle during corners, is reduced with a stiffer body construction. Body roll is decreased to keep the car more level and to preserve the best tire contact with the road, which enhances traction. This improves the car's general handling and cornering capabilities. Studies suggest that increased body stiffness positively affects vehicle handling, ride quality, and stability performance, but there may be an optimal level of stiffness for injury-free performance.[33,34,37,42-44] The relationship between body stiffness and ride comfort is complex. While a stiffer body can improve handling, it can also cause a potentially rougher ride by transferring more road vibrations and impacts to the cabin. However, this can be reduced by carefully planning and fine-tuning the suspension system. The vibrations are absorbed and dampened by a well-designed suspension system, which includes shock absorbers and other parts, resulting in a smoother and more comfortable ride. In order to get the ideal ride comfort, it is essential to balance the body's rigidity with the suspension tune. Studies suggest that body stiffness, flexural mode shapes, and suspension parameters all significantly affect ride comfort, especially in low-frequency ranges.[39,45]

Thus, the model is analyzed by varying the body stiffness (B). Differentiation of lateral, longitudinal, and yaw rates against body stiffness values of 18.6, 28.6, and 48.6, respectively, is observed and depicted in Figs. S19-S21 for a right cornering. Typical passenger vehicles' body stiffness varies between 12 and 30, and hence, the above values are chosen.[30] The longitudinal component shows variations for higher values of B while it remains consistent for the ideal passenger car ranges, and the lateral velocities show variations in the mid-range. The yaw rate has shown consistent and comparable variations for all the values of B, as shown in Fig. S22. Owing to this, the body slip angle plotted against the front angle depicted in Fig. 13 has shown a consistent response in both B=18.6 and 28.6, which is the range of interest. The slip angle has shown variation in its response for large values of B, hinting at the fact that the model is sensitive to higher stiffness values.

4. Conclusion

The designed non-linear, slip-angle-based dynamic vehicle model presents a promising solution for improving on-road illumination, which can ultimately result in improved driving experience and increased safety. The state space model considers the maximum turn angle for both right and left turns to design a compensatory headlamp adjustment model. Although independently designed, the results show that the correction angle for both headlamps is similar, which makes the processing of the model easier. In the permitted body stiffness range for passenger cars, the model exhibits an acceptable response. It should be highlighted, however, that

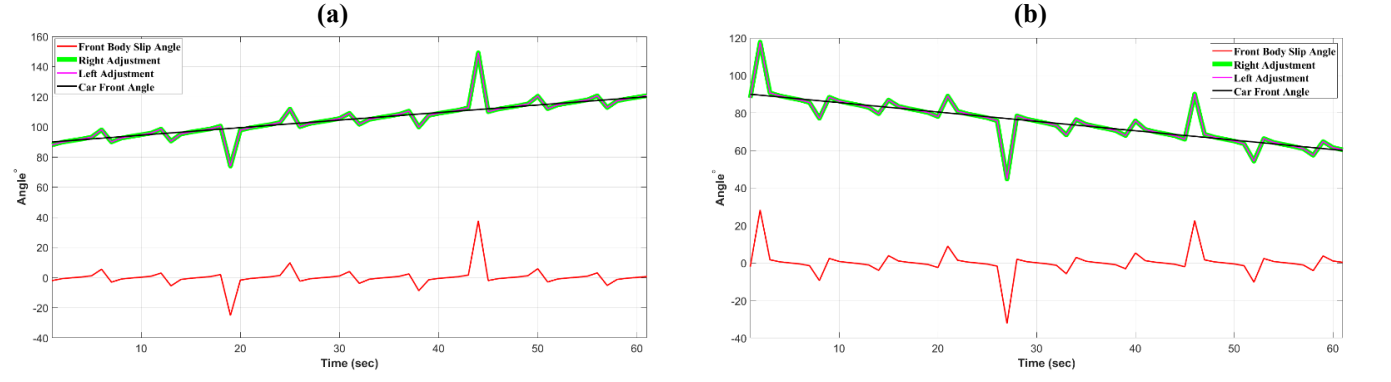

Fig. 12: Right and left headlamp adjustment with respect to Car front angle, calculated slip angle when the vehicle is subjected to a (a) Right turn (b) Left turn.

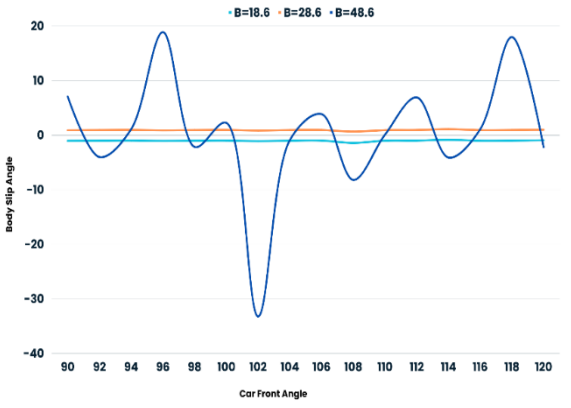

Fig. 13: Body Slip Angle for B=18.6, 28.6 and 48.6.

the model requires more refining to fully capture the complexities of real-world driving conditions, such as variations in weather, road conditions, vehicle load, and driver behavior. Future study can concentrate on investigating these aspects and their possible impact on the model's effectiveness. This will aid in the construction of a more robust and consistent model that can better serve the demands of drivers and improve their road safety.

In addition to the aforementioned considerations, variables such as vehicle speed and suspension system can be investigated for their impact on slip angle computation and, subsequently, headlamp adjustment. These variables could be considered to the model to make it more complete and useful in real-world driving circumstances. In addition, the model might be validated by experimentation and field testing to confirm its robustness and reliability in a variety of configurations. Overall, the dynamic vehicle model based on slip angle has the potential to considerably improve driving safety and comfort by assuring optimal light adjustment and road illumination. The study presented here establishes a foundation for future work aimed at designing and developing an integrated controller that employs sensor technologies for front, center, and rear angle detection, as well as longitudinal and lateral velocity component detection. The model can be modified by taking into account the dynamic load of the vehicle as well as the effect of tire stiffness. The controller predicts body slip angle, allowing for precise headlight beam modulation for increased visibility and vehicle safety. Multiple on-road tests are necessary to confirm the model's effectiveness in real-world scenarios. Future study into the possibility for merging these components into a cohesive controller is an interesting avenue to follow in order to improve vehicle safety and produce more effective and efficient headlight beam adjustment systems.

Conflict of Interest

There is no conflict of interest.

Supporting Information

Applicable.

References

[1] G. Toney, C. Bhargava, Adaptive headlamps in automobile: a review on the models, detection techniques, and mathematical models, *IEEE Access*, 2021, **9**, 87462-87474, doi: 10.1109/ACCESS.2021.3088036.

[2] H. Li, R. Tiwari, V. Pickert, S. Dlay, Fuzzy control for platooning systems based on V2V communication, 2018 International Conference on Computing, Electronics & Communications Engineering (iCCECE). August 16-17, Southend, UK, IEEE, 2018, 247-252, doi: 10.1109/iCCECOME.2018.8658807.

[3] H. Li, H. Wu, I. Gulati, S. A. Ali, V. Pickert, S. Dlay, An improved sliding mode control (SMC) approach for enhancement of communication delay in vehicle platoon system, *IET Intelligent Transport Systems*, 2022, **16**, 958-970, doi: 10.1049/itr2.12189.

[4] H. Li, I. Gulati, S. Stainton, S. A. Ali, V. Pickert, S. Dlay, Sliding Mode Control for Vehicular Platoon based on V2V Communication, Proceedings of the 32nd International Technical Meeting of the Satellite Division of the Institute of Navigation (ION GNSS+ 2019), September 16-20, Miami, Florida, Institute of Navigation, 2019, 2078-2089, doi: 10.33012/2019.16887.

[5] J. Wang, J. Steiber, B. Surampudi, Autonomous ground vehicle control system for high-speed and safe operation, *International Journal of Vehicle Autonomous Systems*, 2009, **7**, 18, doi: 10.1504/ijvas.2009.027965.

[6] E. P. Ping, K. Hudha, H. Jamaluddin, Hardware-in-the-loop simulation of automatic steering control for lanekeeping manoeuvre: outer-loop and inner-loop control design, *International Journal of Vehicle Safety*, 2010, **5**, 35, doi: 10.1504/ijvs.2010.035318.

[7] M. Elbanhawi, M. Simic, R. Jazar, The role of path continuity in lateral vehicle control, *Procedia Computer Science*, 2015, **60**, 1289-1298, doi: 10.1016/j.procs.2015.08.194.

[8] G. V. Raffo, G. K. Gomes, J. E. Normey-Rico, C. R. Kelber, L. B. Becker, A predictive controller for autonomous vehicle path tracking, *IEEE Transactions on Intelligent Transportation Systems*, 2009, **10**, 92-102, doi: 10.1109/TITS.2008.2011697.

[9] A. De Luca, G. Oriolo, C. Samson, Feedback control of a nonholonomic car-like robot. Robot Motion Planning and Control. Berlin, Heidelberg: Springer Berlin Heidelberg, 1998, 171-253, doi: 10.1007/bfb0036073.

[10] Y. Kanayama, Y. Kimura, F. Miyazaki, T. Noguchi, A stable tracking control method for an autonomous mobile robot, *Proceedings., IEEE International Conference on Robotics and Automation*. May 13-18, Cincinnati, OH, USA, IEEE, 1990, 384-389, doi: 10.1109/ROBOT.1990.126006.

[11] H. Dugoff, P. S. Fancher, L. Segel, An Analysis of Tire Traction Properties and Their Influence on Vehicle Dynamic Performance, SAE Technical Paper Series, SAE International, 1970, 1219-1243, doi: 10.4271/700377.

[12] Kiencke and L Nielsen U. Automotive control systems: for engine, driveline, and vehicle, *Measurement Science and Technology*, 2000, **11**, 1828, doi: 10.1088/0957-0233/11/12/708.

[13] E. Frazzoli, M. A. Dahleh, E. Feron, Robust hybrid control

for autonomous vehicle motion planning, Proceedings of the 39th IEEE Conference on Decision and Control. December 12-15, 2000, Sydney, NSW, Australia, IEEE, 2000, 821-826, doi: 10.1109/CDC.2000.912871.
[14] B. Paden, M. Čáp, S. Z. Yong, D. Yershov, E. Frazzoli, A survey of motion planning and control techniques for self-driving urban vehicles, *IEEE Transactions on intelligent vehicles*, 2016, **1**, 33-55, doi: 10.1109/TIV.2016.2578706.
[15] K. N. Murphy, Analysis of robotic vehicle steering and controller delay, 5th International Symposium on Robotics and Manufacturing, 1994, 631-636.
[16] T. Hellstrom, O. Ringdahl, Follow the Past: a path-tracking algorithm for autonomous vehicles, *International Journal of Vehicle Autonomous Systems*, 2006, **4**, 216, doi: 10.1504/ijvas.2006.012208.
[17] R. Gockley, J. Forlizzi, R. Simmons, Natural person-following behavior for social robots, Proceedings of the ACM/IEEE International Conference on Human-Robot Interaction, Arlington Virginia USA, ACM, 2007, 17-24, doi: 10.1145/1228716.1228720.
[18] J. Wit, C. D. Crane III, D. Armstrong, Autonomous ground vehicle path tracking, *Journal of Robotic Systems*, 2004, **21**, 439-449, doi: 10.1002/rob.20031.
[19] Y. Kuwata, J. Teo, S. Karaman, G. Fiore, E. Frazzoli, J. How, Motion Planning in Complex Environments Using Closed-loop Prediction, AIAA Guidance, Navigation and Control Conference and Exhibit. Honolulu, Hawaii, AIAA, 2008: AIAA2008-7166, doi: 10.2514/6.2008-7166.
[20] S. Thrun, M. Montemerlo, H. Dahlkamp, D. Stavens, A. Aron, J. Diebel, P. Fong, J. Gale, M. Halpenny, G. Hoffmann, K. Lau, C. Oakley, M. Palatucci, V. Pratt, P. Stang, S. Strohband, C. Dupont, L.-E. Jendrossek, C. Koelen, C. Markey, C. Rummel, J. van Niekerk, E. Jensen, P. Alessandrini, G. Bradski, B. Davies, S. Ettinger, A. Kaehler, A. Nefian, P. Mahoney, Stanley: the robot that won the DARPA grand challenge, *Journal of Field Robotics*, 2006, **23**, 661-692, doi: 10.1002/rob.20147.
[21] F. N. Martins, W. C. Celeste, R. Carelli, M. Sarcinelli-Filho, T. F. Bastos-Filho, An adaptive dynamic controller for autonomous mobile robot trajectory tracking, *Control Engineering Practice*, 2008, **16**, 1354-1363, doi: 10.1016/j.conengprac.2008.03.004.
[22] Gillespie, T. D., Fundamentals of vehicle dynamics, Society of Automotive Engineers, Warrendale, PA, USA, 1992, 1-22,doi: 10.4271/r-114.
[23] K. Takikawa, Y. Atsumi, A. Takanose, J. Meguro, Vehicular trajectory estimation utilizing slip angle based on GNSS Doppler/IMU, *ROBOMECH Journal*, 2021, **8**, 5, doi: 10.1186/s40648-021-00195-4.
[24] K. B. Singh, Vehicle sideslip angle estimation based on tire model adaptation, *Electronics*, 2019, **8**, 199, doi: 10.3390/electronics8020199.
[25] D. Selmanaj, M. Corno, G. Panzani, S. M. Savaresi, Vehicle sideslip estimation: A kinematic based approach, *Control Engineering Practice*, 2017, **67**, 1-12, doi: 10.1016/j.conengprac.2017.06.013.
[26] H. Du, J. Lam, K.-C. Cheung, W. Li, N. Zhang, Side-slip angle estimation and stability control for a vehicle with a non-linear tyre model and a varying speed, *Proceedings of the Institution of Mechanical Engineers*, *Part D: Journal of Automobile Engineering*, 2015, **229**, 486-505, doi: 10.1177/0954407014547239.
[27] D. W. Pi, N. Chen, J. X. Wang, B. J. Zhang, Design and evaluation of sideslip angle observer for vehicle stability control, *International Journal of Automotive Technology*, 2011, **12**, 391-399, doi: 10.1007/s12239-011-0046-4.
[28] C. Huang, Y. Tung, H. Lu, T.J.Yeh, Balancing control of a bicycle-riding humanoid robot with center of gravity estimation, *Advanced Robotics*, 2018, **32**, 918-929, doi: 10.1080/01691864.2018.1509017
[29] L. Khera, N. Kumar, A. Maurya, Study of aerodynamics on Indian budget concept car, *International Journal of Vehicle Structures and Systems*, 2021, **12**, 521-525, doi: 10.4273/ijvss.12.5.07.
[30] M. K. Pradhan, J. K. Verma, S. K. Jain, Kunal, H. Pariyar, R. Das, Comparative aerodynamics analysis of maruti suzuki alto models. Advances in Fluid Dynamics. Singapore: Springer Singapore, 2020, 589-604, doi: 10.1007/978-981-15-4308-1_46.
[31] G. Siva, V. Loganathan, Design and aerodynamic analysis of a car to improve performance, *Middle-East Journal of Scientific Research*, 2016, **24**, 133-140, doi: 10.5829/idosi.mejsr.2016.24.RIETMA121.
[32], R. B. Sharma, CFD simulation for flow over passenger car using tail plates for aerodynamic drag reduction, *IOSR Journal of Mechanical and Civil Engineering*, 2013, **7**, 28-35, doi: 10.9790/1684-0752835.
[33] O. Danielsson, A, G. Cocaña, Influence of body stiffness on vehicle dynamics characteristics in passenger cars, Masters thesis in Automotive Engineering-Chalmers University of Technology, Sweden, 2015, 1-82.
[34] K. Guo, Y. Kong, Vehicle dynamics: Theory and application, CRC Press, 2017, ISBN: 978-3-031-74458-7.
[35] V. Arvind, Optimizing the turning radius of a vehicle using symmetric four-wheel steering system, *International Journal of Scientific & Engineering Research*, 2013, **4**, 2177-2184.
[36] H. F. Grip, L. Imsland, T. A. Johansen, J. C. Kalkkuhl, A. Suissa, Vehicle sideslip estimation, *IEEE control systems magazine*, 2009, **29**, 36-52, doi: 10.1109/MCS.2009.934083.
[37] D. Gong, W. Sun, J. Zhou, X. Xie, Analysis on the vertical coupled vibration between bogies and metro car body, *Procedia Engineering*, 2011, **16**, 825-831, doi: 10.1016/j.proeng.2011.08.1161.
[38] D. Younesian, S. R. Marjani, E. Esmailzadeh, Importance of flexural mode shapes in dynamic analysis of high-speed trains traveling on bridges, *Journal of Vibration and Control*, 2014, **20**, 1565-1583, doi: 10.1177/1077546312466882.
[39] L. X. Long, L. V. Quynh, B. V. Cuong, Study on the influence of bus suspension parameters on ride comfort, *Vibroengineering Procedia*, 2018, **21**, 77-82, doi: 10.21595/vp.2018.20271.
[40] P. E. Pfeffer, M. Harrer, D. N. Johnston, Interaction of

vehicle and steering system regarding on-centre handling, *Vehicle System Dynamics*, 2008, **46**, 413-428, doi: 10.1080/00423110701416519.
[41] M. Ahmadian, W. Huang, A qualitative analysis of the dynamics of self-steering locomotive trucks, *Vehicle System Dynamics*, 2002, **37**, 85-127, doi: 10.1076/vesd.37.2.85.3537.
[42] K. C. Kim, C. M. Kim, Analysis process applied to a high stiffness body for improved vehicle handling properties, *International Journal of Automotive Technology*, 2012, **8**, 629-636.
[43] K. C. Kim, C. M. Kim, A study on the development of high stiffness body for suspension performance, *Transactions of the Korean Society for Noise and Vibration Engineering*, 2005, **15**, 799-805, doi: 10.5050/ksnvn.2005.15.7.799.
[44] R. J. Butler, H. P. Crowell, I. M. Davis, Lower extremity stiffness: implications for performance and injury, *Clinical Biomechanics*, 2003, **18**, 511-517, doi: 10.1016/S0268-0033(03)00071-8.
[45] D. Gong, W. Sun, J. Zhou, X. Xie, Analysis on the vertical coupled vibration between bogies and metro car body, *Procedia Engineering*, 2011, **16**, 825-831, doi: 10.1016/j.proeng.2011.08.1161.